

Modular Hydrogel–Mesoporous Silica Nanoparticle Constructs for Therapy and Diagnostics

Melanie Gerstenberg, Christina M. Stürzel, Tanja Weil, Frank Kirchoff, and Mika Lindén*

Self-assembled peptide fibrils are abundant in *in vivo* systems and have been associated both with normal physiological functions and with different diseases. Herein, a proof-of-concept study is presented, where aggregates of synthetic, fibril-forming peptides are studied as carriers for mesoporous silica nanoparticles (MSNs), giving a hydrogel@MSN hybrid structure. It is shown that when the peptide carries a cellular-targeting motif, in this case arg-gly-asp (RGD), the fibrillar aggregates efficiently attach to cancer cells, and the attached MSNs can then be locally taken up by the cells and intracellularly release their cargo or release their cargo close to the outer membrane of the cells. If the targeting motif is not present on the fibrils, hardly any attachment of the fibrillar aggregates to the target cells occurs. The higher drug carrying capacity of the MSNs together with the efficient cellular attachment of the fibrillar aggregates represents a synergistic approach toward reaching a modular drug release system, bringing together the strengths of each component of the system. Finally, it is noted that although the experimental design is such that the fibrillar aggregates would not be capable of entering cells due to their large size, the approach would also be applicable to smaller fibrillar aggregates.

1. Introduction

Depending on their amino acid sequence, peptides may self-assemble into fibrils several micrometers in length and with a cross-section diameter of 10–20 nm. Side chain–side chain interactions across neighboring β -strands are a key determinant of fibril formation and their self-propagating ability. The fibrils can further aggregate to form hydrogel-type micro- or macrostructures.^[1–4] Peptide self-assembly has also been closely associated with different diseases. For example, the aggregation of β -amyloid ($A\beta$) peptides in brain tissue is associated with Alzheimer's disease (AD).^[5,6] However, accumulating evidence suggests that the protofibrils, rather than the fully grown fibrils, cause the disease.^[7] Furthermore, peptidefibrils may also play a role in sexual transmission of HIV infection.^[8,9] Naturally occurring fragments of the abundant semen marker prostatic acidic phosphatase (PAP) forms amyloid

fibrils. These fibrils, termed Semen-derived Enhancer of Virus Infection (SEVI), capture HIV particles and promote their attachment to target cells, thereby enhancing the infectious virus titer by several orders of magnitude in limiting dilution analyses.^[9] Recently, functional amyloids have been discovered where amyloids are implicated in performing normal physiological functions of the host organism rather than creating diseases. Thus, spermamyloids participate in the selection and release of sperm,^[10] while fibrillar structures of Pmel17 found on the melanosomes of mammals seem to act as a template for melanin synthesis.^[11] Moreover peptide hormones as the gonadotropin releasing hormone (GnRH) are often stored by the body in secretion granules with amyloid-like structures.^[12] In addition, self-assembled peptide aggregates can also have positive therapeutic influences. We have recently demonstrated that amyloid-forming synthetic peptides enhance nerve regeneration *in vivo* without inducing toxicity.^[13] The ability of amyloids to interact with the cell membrane and other small biomolecules exhibits great potential to be used as a biomaterial for cell adhesion and for boosting retroviral gene delivery and provides a rapid means for concentrating viruses.^[14] It was recently shown that amyloids of α -synuclein and amyloid of poly-L-lysine can interact with lentiviral particles and enhance transduction efficiency in cells.^[15] Cationic β -lactoglobulin amyloid fibrils were reported to enhance

M. Gerstenberg, M. Lindén
Institute of Inorganic Chemistry II
University Ulm
Albert-Einstein-Allee 11, 89081 Ulm, Germany
E-mail: mika.linden@uni-ulm.de

C. M. Stürzel, F. Kirchoff
Institute of Molecular Virology
Ulm University Medical Center
Meyerhofstrasse 1, 89081 Ulm, Germany

T. Weil
Department for Synthesis of Macromolecules
Max-Planck-Institute for Polymer Research
Ackermannweg 10, 55128 Mainz, Germany

 The ORCID identification number(s) for the author(s) of this article can be found under <https://doi.org/10.1002/anbr.202100125>.

© 2021 The Authors. Advanced NanoBiomed Research published by Wiley-VCH GmbH. This is an open access article under the terms of the Creative Commons Attribution License, which permits use, distribution and reproduction in any medium, provided the original work is properly cited.

DOI: 10.1002/anbr.202100125

the transport of metal nanoparticles into cells.^[15] These results are in line with the importance of peptide charge for efficient attachment to cellular membranes,^[16] and most antimicrobial peptides carry a high positive charge.^[17,18] Hydrogels based on self-assembling peptides have also extensively been studied for tissue engineering applications, and hydrogels in combination with MSN have also been studied for transdermal drug administration.^[19] We recently showed that macroscopic, injectable, self-assembling hybrid nanoparticle–peptide hydrogels based on the charge-neutral RADA-16-I and mesoporous silica nanoparticles (MSNs) are promising materials for cell-directed delivery of bioactives to stem cells present inside the hydrogel *in vitro*.^[20] MSNs are promising drug carrier platforms, as they exhibit a large mesopore volume, and a high surface area, making it possible to reach high drug loading in the range of 35 wt%.^[21] Furthermore, they can be easily surface functionalized, allowing both the drug–carrier and the nanoparticle–bioenvironment interactions to be independently optimized.^[21,22] In addition, they are biocompatible and biodegradable and are mainly renally excreted from the body.^[23,24] A recent review summarizes the current progress in relation to clinical translation of silica nanoparticles.^[25] Cells present inside the hydrogel could internalize the MSNs through endocytosis, and small hydrophobic drugs present inside the mesopore system of the MSNs can be delivered intracellularly.^[26] The cells did not seem to internalize the anionic, fibril-forming RADA-I peptide,

again highlighting the importance of peptide charge for modulating cellular uptake. However, cells coadministered with the MSNs immediately internalized MSNs irrespective of the surface charge or type of surface functionalization.

Inspired by these results, we hypothesized that the hydrogel particles could serve as potent carriers for MSNs, as schematically shown in **Figure 1**. If the attractive peptide fibril–MSN interactions are strong enough and the aggregates large enough, MSNs' uptake can be delayed even hindered, and the MSNs rather serve as drug depots for extracellular delivery (Scheme I). This is important especially in cases where the drug should act on the outer cellular membrane, like for small-molecule drugs as well as for peptides or proteins that interact with G protein-coupled receptors or ion channels. Furthermore, if the self-assembling peptide is carrying a targeting ligand, it could also serve as a cell-specific carrier system, and especially so for anionic hydrogel-forming peptides, for which the unspecific adsorption to the cells is generally lower than for cationic counterparts. Local injection of the hydrogel aggregates would then allow the aggregates to accumulate on target cells, and drug-containing MSNs could either be coadministered or postadministered and attach to the hydrogel aggregates. If the water solubility of the drug is low, detachment of MSNs with time followed by particle uptake by the cells could be used for intracellular drug delivery to the target cells, where the fibril

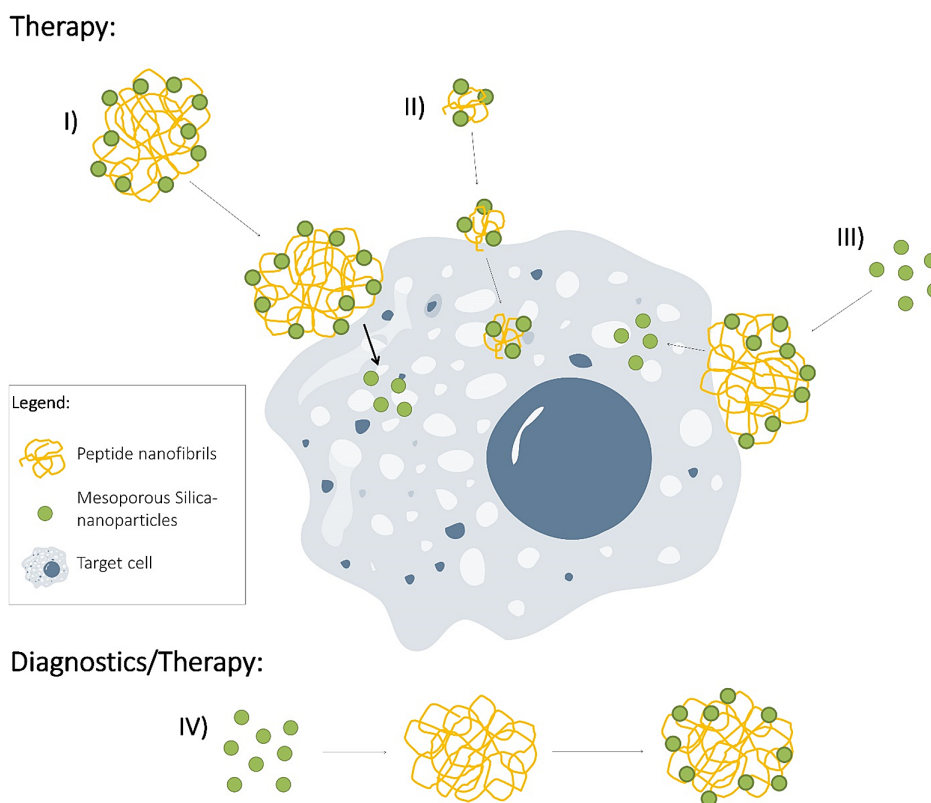


Figure 1. Different hypothetical ways of how hydrogel particles could serve as potent carriers for MSNs. I) If the aggregates are large enough and the peptide fibril–MSN interaction is strong enough, cellular uptake of the MSNs can be delayed. Thus, the MSN may serve as a drug depot for extracellular delivery. II) Smaller aggregates with a size in the 100 nm range could even be internalized by cells for efficient delivery. III) Furthermore, the fibril aggregates can initially be targeted to the cells. MSNs are added in a later stage and can accumulate at the cell interface. IV) An additional strategy that does not involve targeting to cells but which can be used for diagnosis of diseases involving fibrils by attachment of the MSN to fibrillar structures.

aggregates serve both as targeting moieties and allow for a high local concentration of MSNs. Furthermore, if the size of the peptide fibril–MSN aggregate is in the 100 nm range, it could even be internalized by cells (Scheme II). In addition, fibril aggregates can initially be targeted to cells, and MSNs introduced after fibril attachment to the target cells could then be accumulated at the cell interface (Scheme III). Finally, a similar strategy not involving targeting to cells can be used for diagnosis of diseases involving fibrils (Scheme IV).

Two fibril-forming peptides, KFKFEFEEF (PEP), being charge neutral under physiological conditions, and the anionic KFKFEFEEFGGRGDS (PEP_{RGD}), were synthesized via solid-phase peptide synthesis, followed by physisorption of MSNs to the fibril aggregates. As discussed earlier, a neutral or anionic peptide was chosen to minimize peptide fibril-induced cell membrane destabilization and cellular internalization of the fibrils. The cell attachment of these hybrid particles to the human lung cancer cell line A549 was then studied *in vitro*. Finally, the mechanistic aspects of the delivery of the hydrophobic model drug to the cells were investigated, giving proof for the functionality of the developed system.

2. Results and Discussion

2.1. Particle Synthesis and Functionalization

Mesoporous silica particles were prepared according to a modified procedure of the synthesis described by Rosenholm et al.^[26] using cetyltrimethylammonium bromide as the structure-directing agent, resulting in MSNs with cylindrically shaped pores. The MSNs exhibited a narrow particle size distribution with a mean size of around 150 nm, as determined by image analysis of transmission electron microscopy (TEM) images. A TEM image of MSN_{COOH} is exemplarily shown in Figure 2. Also shown in Figure 2 is the nitrogen adsorption isotherm measured for the same particles. A narrow pore-filling step at a relative pressure of around 0.25 p/p_0 hints a relatively narrow pore size distribution, and nonlocal density functional theory (NLDFT) analysis gives a mean mesopore diameter of 3.2–3.3 nm, which is a typical value for such particles. The Brunauer, Emmett, and Teller (BET) areas for all particles were

in the range of 900–1000 $m^2 g^{-1}$, which also is in good agreement with literature values.^[27,28] All three particles were fully dispersible in water (pH = 5.5, 1 mM KCl) with hydrodynamic radii of 206 ± 3 nm (MSN_{OH}), 188 ± 5 nm (MSN_{COOH}), and 215 ± 2 nm (MSN_{NH2}). Thermogravimetric analyses suggested that the concentration of functional groups equaled 1.5 nm^2 for –NH₂ and 0.44 nm^2 for –COOH functions.

The hydrodynamic radii measured for the different MSNs in 1 mM KCl (pH = 5.5) were 188 nm (MSN_{COOH}), 206 nm (MSN_{OH}), and 251 nm (MSN_{NH2}), respectively, showing that all particles were dispersible in water, but the MSN_{COOH} particles showed the highest level of dispersability of the studied particles under the given conditions. The zeta-potential measured under the same conditions was +29 mV for the starting MSN_{NH2} particles but decreased as expected to –12 mV after calcination (MSN_{OH}). Further carboxylation of these particles caused a further decrease in the zeta-potential to –34 mV (MSN_{COOH}). The clearly more negative zeta-potential measured for MSN_{COOH} as compared with MSN_{OH} particles probably results from a combination of the deprotonated carboxylic acid groups and a higher surface silanol concentration of the MSN_{COOH} particles as compared with the MSN_{OH} particles, as the degree of surface hydroxylation should increase for the MSN_{OH} particles during the aqueous functionalization step, leading to MSN_{COOH} particles.

2.2. Peptide Synthesis and Fibril Formation

The peptides KFKFEFEEF (PEP) and KFKFEFEEFGGRGDS (PEP_{RGD}) were synthesized via solid-phase peptide synthesis. The primary sequence of PEP was selected to form fibrils with a net-neutral charge. Matrix-assisted laser desorption/ionization–time of flight mass spectrometry (MALDI-TOF-MS) analyses gave molecular weights of 1121 Da for the PEP peptide, and 1651 Da for the PEP_{RGD} peptide, (see Figure S1, Supporting Information), and these values are in full agreement with the expected peptide molecular masses. The amphipathic basic body of the peptide sequences enables the peptides to self-assemble into fibrillar β -sheet structures in aqueous medium.^[29] In our case, we let the fibrils form overnight in a sodium phosphate buffer (20 mM; pH = 7.0) at a peptide concentration of 0.65 mM. Uranyl acetate staining was used to allow for

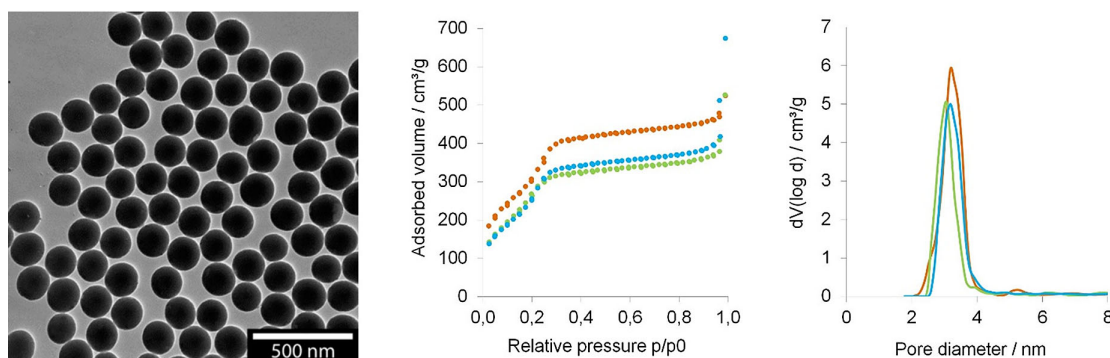


Figure 2. Transmission electron microscopy image of MSN_{OH} particles (left), nitrogen sorption isotherm of the different functionalized particles (middle) and pore size distribution calculated via nonlinear density functional theory (NL-DFT) of all MSN (right) (MSN_{OH}: orange; MSN_{COOH}: green; MSN_{NH2}: blue).

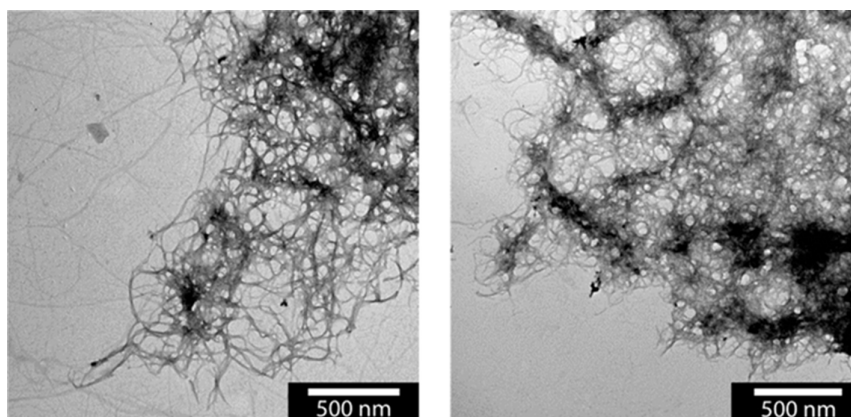


Figure 3. TEM images of the peptide nanofibrils after incubation of PEP (left) and PEP_{RGD} (right) overnight in phosphate-buffered saline (PBS). The fibrils were stained with 2% uranyl acetate for 2 min for a better contrast.

detailed visualization of the obtained fibrillary aggregates by TEM after freeze drying, and representative images are shown in **Figure 3**. Both peptides form long fibrils, which assemble to larger aggregates, where the rim of the aggregates has a more open structure than the internal parts. Aggregate diameters exceeding several micrometers were reached within an hour, making these aggregates large enough not to be internalizable by cells. A high degree of β -sheet formation was verified for both peptides by intercalation of Proteostat (see Figure S2, Supporting Information). The zeta-potential of the PEP fibrillar aggregates measured in 1 mM KCl (pH = 5.5) was 3 ± 1 mV. PEP_{RGD} showed a more negative zeta-potential of -16 ± 1 mV caused by the additional presence of the arg-aspar (RGDS) sequence.

2.3. Noncovalent MSN Attachment to Peptide Nanofibrils

The adsorption of the three different MSNs onto preformed fibrillar PEP and PEP_{RGD} aggregates from sodium phosphate buffer (20 mM; pH = 7.0) was first studied by TEM imaging of particle–fibril aggregates isolated by freeze drying. The particles were preincubated with the different fibrils for 45 min at room temperature at a concentration of 150 $\mu\text{g MSNs}/\mu\text{mol peptide}$ before freeze drying. The corresponding images are shown in **Figure 4**. The most homogeneous MSN distribution was observed for MSN_{COOH} particles, while strongly aggregated MSNs and particle-free fibrillar aggregates coexisted with mixed MSN–fibrillar aggregates for MSN_{OH} and MSN_{NH₂}. The relatively strong aggregation of MSN_{NH₂} particles is in line with their

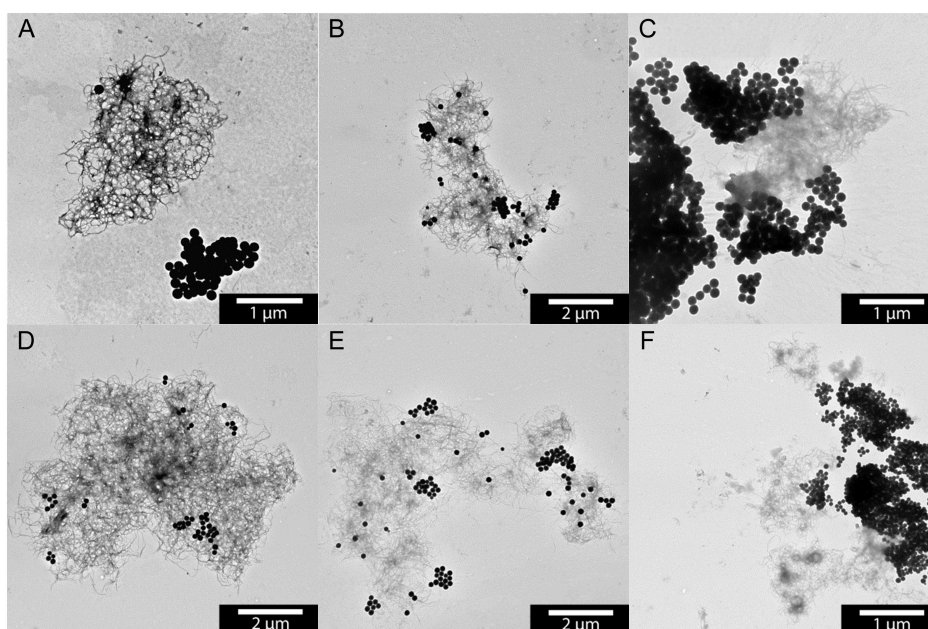


Figure 4. A,D) TEM images of the noncovalent attachment of the MSN_{OH}, B,E) MSN_{COOH}, and C,F) MSN_{NH₂} particles to the peptide nanofibrils PEP. Fibrils were preincubated in sodium phosphate buffer (20 mM; pH = 7.0) overnight before particles were attached ($150 \mu\text{g } \mu\text{mol}^{-1}$ peptide) for 45 min at RT. To get a higher contrast, the TEM grids were stained with 2% uranyl acetate for 2 min before imaging.

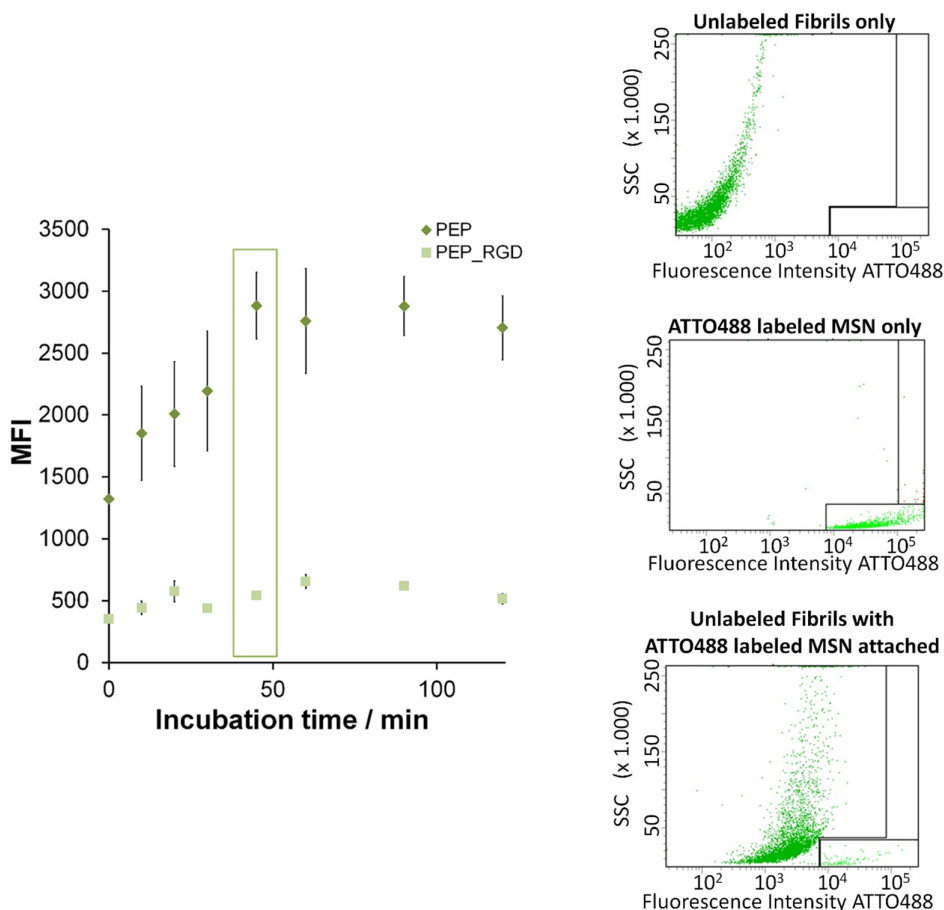


Figure 5. Kinetics of the MSN_{COOH} attachment to the peptide nanofibrils PEP and PEP_{RGD} measured via flow cytometry (left). Exemplary FACS maps for fibrils, particles, and fibril–MSN aggregates after an incubation time of 90 min (right). Unlabeled PEP fibrils were detected as events, while the non-covalently attached ATTO488 fluorescent labeled MSN_{COOH} leads to an increase in fluorescence of the fibrillar aggregates.

low absolute zeta-potential value of -11 mV measured at pH 7.4, leading to fast aggregation of the particles. Thus, the high negative charge of the MSN_{COOH} particles hindered particle aggregation, and the physisorption of the particles to fibril aggregates was probably driven by a combination of hydrogen bonding and apolar interactions. For this reason, MSN_{COOH} was chosen for further experiments.

The kinetics of MSN_{COOH} attachment to the two different types of fibrils was evaluated by flow cytometry (fluorescence-activated cell sorting [FACS]) measurements using ATTO488 fluorescently labeled MSN_{COOH} particles. The incubation time was varied between 0 and 120 min, and the conditions were otherwise identical to those described earlier. The results are shown in **Figure 5**. The particle attachment starts directly after addition of the particles to the fibrils and saturates after an incubation time of about 45 min. The particle adsorption resulted in a higher signal for the PEP fibrils compared with the PEP_{RGD} ones—what can be caused by an lesser particle adsorption in the case of PEP_{RGD} caused by repulsive interactions between the more negatively charged fibrils and the carboxylic acid-functionalized particles or by differences in the size and density of the fibril aggregates.

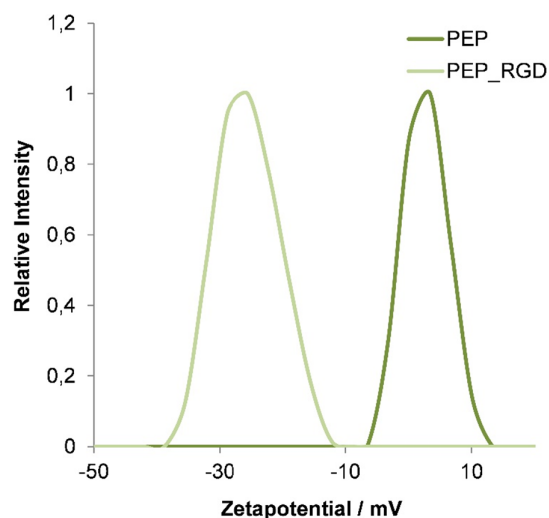


Figure 6. Zeta-potential intensity distribution of the peptide nanofibrils after incubation of PEP and PEP_{RGD} for 24 h in PBS and diluted with 1 mM KCl (pH = 5.5).

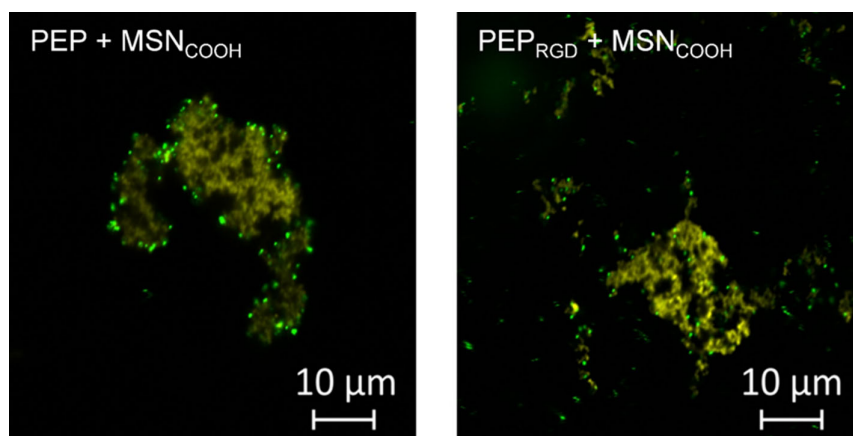


Figure 7. Confocal fluorescence microscopy images of the PEP (left) and PEP_{RGD} fibrils (right) (10 mol% ATTO647N labeled) with 45 min noncovalently attached MSN_{COOH} (ATTO488 labeled) (yellow: fibrils; green: MSN_{COOH}).

To evaluate the presence of any free particles at the time point of 45 min, zeta-potential measurements were performed. The zeta-potential intensity distributions are shown in **Figure 6**. For both types of fibrils, there is only one local maximum detectable, which has a mean value lower than for the pure fibrils caused by the attachment of the highly negatively charged MSN_{COOH}. The absence of a second local maximum at around -34 mV suggests that there are very few, if any, free particles left in solution, excluding an incomplete particle adsorption as a reason for lower amounts of particles per fibril aggregate for PEP_{RGD}.

The distributions of the MSNs in the peptide nanofibrillar aggregates were further studied by confocal fluorescence microscopy, and the results are shown in **Figure 7**. To allow detection also of the peptide fibrils by fluorescence microscopy, PEP and

PEP_{RGD} were covalently labeled with ATTO647N-NHS-ester. The labeled peptides were diluted with unlabeled peptide stock solution to achieve 10 mol% labeled peptide stock solutions. No particle-free fibril aggregates were detected, giving further support for virtually complete physisorption of MSN_{COOH} particles to the fibrillar aggregates. In addition, the confocal images show a preferential localization of the particles at the outer surface of the peptide nanofibrils aggregates, in agreement with findings related to virus particles interacting with peptide nanofibrils reported earlier.^[14]

Finally, due to their large size, the fibril–MSN aggregates sedimented over a timescale of hours. However, gentle shaking of the sample vessel was enough to fully redisperse the aggregates.

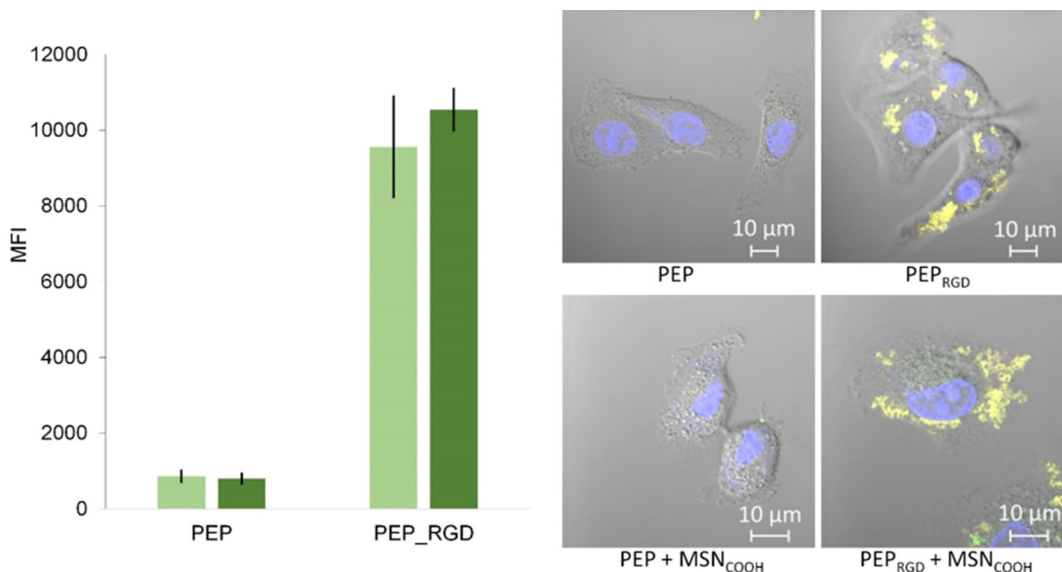


Figure 8. Measurements of the PEP and PEP_{RGD} fibril (attachment to the A549 cell line after 3 h incubation at 37 °C without [light green] and with [dark green] noncovalently attached MSN_{COOH} via flow cytometry [left] and confocal fluorescence microscopy [blue: cell core; yellow: fibrils] [right]). Fibrils were allowed to form in a 10% ATTO647N-labeled peptide stock solution overnight, after which unlabeled MSN_{COOH} particles were allowed to attach to the fibrillar aggregates for 45 min at room temperature.

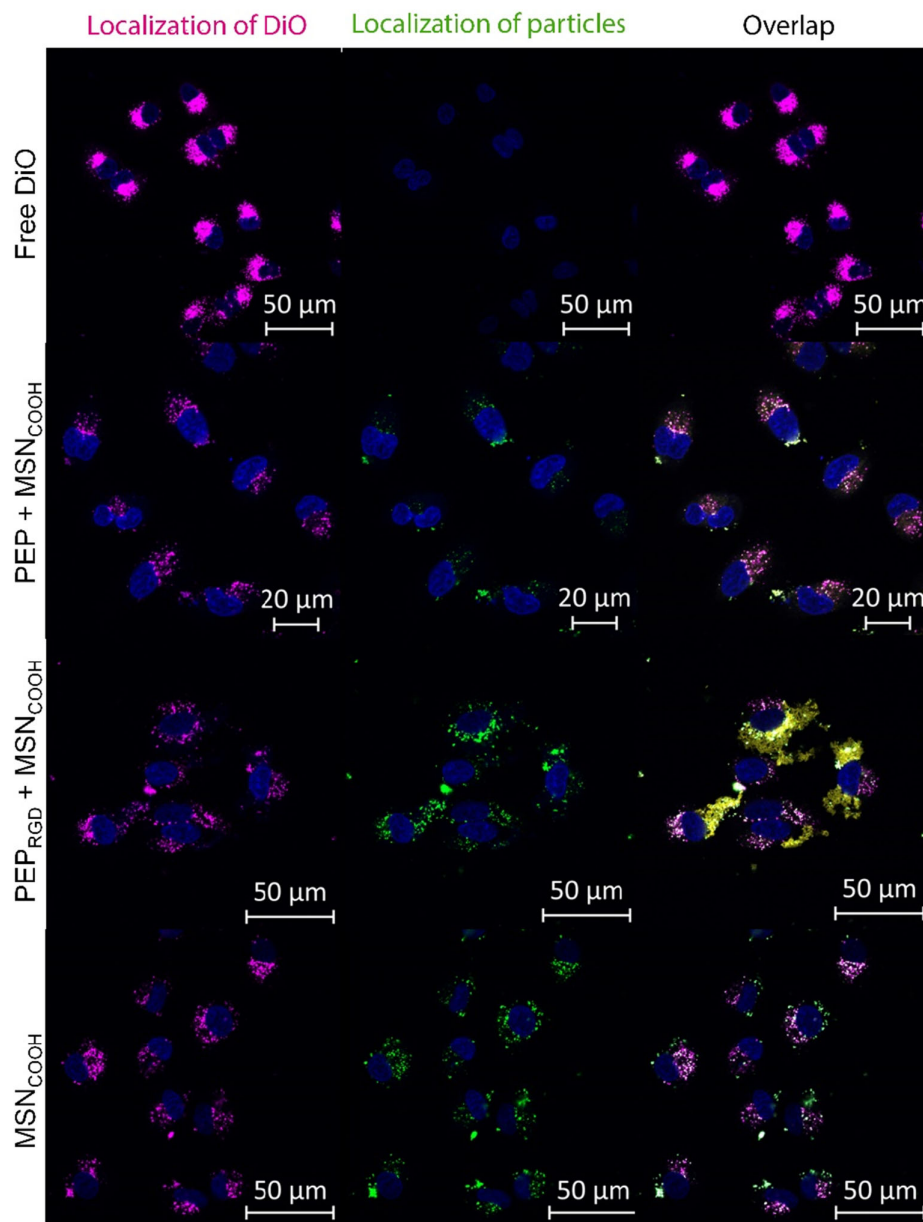


Figure 9. MSN_{COOH} and DiO localization after 24 h incubation with A549 cells as studied by confocal fluorescence microscopy at 37 °C. The cell cores were stained with Hoechst (blue), the particles with ATTO565 (green), the fibrils with ATTO647N (yellow), and DiO is fluorescent by itself (pink).

2.4. Cytocompatibility and Cell Attachment

Potential *in vitro* cell toxicity was assessed using the Cell Titer Glo-assay. A549 cells were exposed to either fibrils alone (26 μM), fibrils with attached particles (26 μM; 150 μg MSN_{COOH}/μmol peptide), or just particles (50 μg mL⁻¹) and incubated for either 24 or 48 h. The fibril concentration was set to 26 μM because this concentration was used in later cell experiments described in more detail below. No influence on cell viability was observed for any of the studied combinations, indicative of high cytocompatibility of all studied systems (see Figure S3, Supporting Information).

For evaluation of the cellular attachment of the MSN–fibrillar aggregates to cells, particles were preadsorbed onto ATTO647N-labeled fibrillar aggregates, and the hybrid aggregates were incubated for 3 h with adenocarcinomic human alveolar basal epithelial (A549) cells at 37 °C in medium containing 10% serum. A549 cells were chosen as they overexpress receptors against the RGD peptide.^[30] As control, the attachment of particle-free fibrillar aggregates was also studied. FACS and confocal fluorescence microscopy results are given in **Figure 8**. The FACS results show a clearly higher attachment of the PEP_{RGD} fibrillar aggregates to the cells in comparison with the PEP fibrillar aggregates, while the presence or not of particles did not influence the extent of

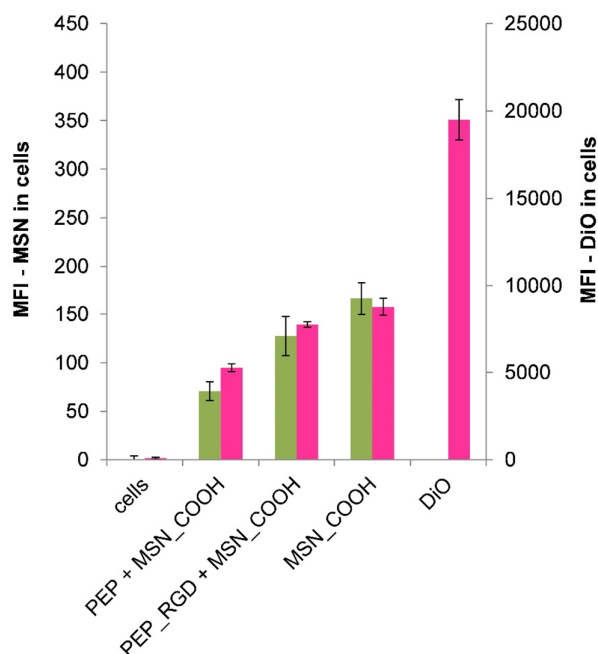


Figure 10. Detection of the ATTO488-labeled MSN_{COOH} inside the cells after 24 h incubation at 37 °C via flow cytometry (green). Fluorescence of extracellular located particles was quenched by incubating the cells with trypan blue for 15 min before measurement. For a better signal, a particle concentration of 250 μg μmol⁻¹ peptide was used. Detected DiO fluorescence in cells after 24 h at 37 °C (pink).

attachment. This indicates that chemical modification of the peptides with the RGD targeting sequence strongly enhances the fibrillar aggregate adhesion to the outer membrane of A549 cells. The difference in cell attachment between the two peptides cannot be ascribed to differences in their zeta-potential values, as the neutral PEP fibrils could be expected to be attached more strongly to the cells than the more negatively charged PEP_{RGD}. Therefore, some active targeting seems to take place. The confocal microscopic investigations verify these results. There are large PEP_{RGD} aggregates attached to the outer membrane of the A549 cells, while no attachment was detectable for PEP fibrils. Even after 3 h incubation, the particles stay distributed at the fibril aggregates. The fibrillar aggregates were not internalized by the cells, and there was also no indication of uptake of peptides that potentially could detach from the fibrils in contact with the cells, even if some sedimentation of the micrometer-sized particle–fibril aggregates that could increase the concentration of aggregates close to the cellular surface could be effective. Also for MSNs, the absolute majority of the particles remained attached to the fibrillar aggregates at this time point, and little or no uptake of MSNs by the cells could be seen. Thus, these results imply that an active targeting of MSN–fibrillar aggregates to cells seems plausible. MSNs can then be positioned in close proximity to the target cells, but their uptake kinetics is strongly kinetically hindered due to their strong attractive interactions with the peptide fibrils. Thus, diffusion/particle dissolution-controlled release of drugs in the proximity of the outer cellular membrane seems feasible.

2.5. Loading and Release of a Hydrophobic Model Drug

To evaluate the drug delivery potential and to study the mechanism of delivery, ATTO565 dye-labeled MSN_{COOH} particles were loaded with a hydrophobic small-molecule model drug, the green fluorescent 3,3'-dioctadecyloxycarbocyanine (DiO) (75 ng DiO/mg MSN_{COOH}). This dye has been successfully employed as a model drug in previous studies.^[31–33] It has been shown to have limited leakage out of the MSNs under biologically relevant conditions,^[33] which should allow the potential influence of MSN internalization by the cells to be evaluated. The particles were loaded by DiO through adsorption from cyclohexane, and UV/vis spectroscopy analysis of the supernatant after loading indicated quantitative adsorption of DiO into MSNs (see Figure S4, Supporting Information).

The nonrelease of DiO from MSNs into water was also demonstrated (see Figure S5, Supporting Information) and was independent of solution pH. Therefore, if DiO is detected inside cells, it should mainly be an indication of intracellular release of DiO from MSNs that have been internalized by the cells.

Free DiO and MSNs containing DiO were used as controls. After adsorption of the DiO-containing MSNs to ATTO647N dye-labeled fibrils, the hybrid aggregates were added to A549 cells and incubated for 3 h at 37 °C in 10% serum-containing medium (see Figure S6, Supporting Information). Only in the case of free DiO, fluorescence originating from DiO could be detected intracellularly at this time point. For the DiO-loaded MSN_{COOH} particles, the DiO fluorescence colocalized with that of the particles and was found to be extracellular. This was the case both in the presence and in the absence of fibrils, indicating that the uptake kinetics of the strongly negatively charged MSN_{COOH} is much slower than that previously observed for positively charged MSNs for other types of cells *in vitro*.^[34–36] The incubation time was therefore extended to 24 h, and the results are summarized in Figure 9. For the free DiO, a clear DiO fluorescence was detected around the cell nucleus, while a pronounced colocalization of fluorescence originating from DiO and MSNs inside intracellular compartments was observed for free MSNs containing DiO. Large differences could be seen between the different hybrid MSN–fibril systems. For MSN–PEP_{RGD}, a very high particle-related fluorescence and colocalized DiO fluorescence were found, even to an extent that the particle fluorescence intensity was higher than that observed for the free particles. For the MSN–PEP system, in contrast, hardly any particle-related fluorescence could be observed intracellularly. In this case, the DiO fluorescence intensity was also lower as compared with that observed for the MSN–PEP_{RGD} system and even lower than that observed for the free particles. Flow cytometric measurements of the relative amounts of particles and DiO inside the cells substantiate these observations. For these measurements, ATTO488-labeled particles as well as the hybrid aggregates of fibrils and ATTO488-labeled MSN_{COOH} were incubated with the A549 cells for 3 h at 37 °C. After washing away all free particles and aggregates with PBS, the cells were incubated for 15 min at room temperature (RT) with a Trypan blue solution (0.5 mg mL⁻¹ in PBS) to quench the fluorescence of the extracellularly located particles. For these experiments, the particle concentration was increased to 250 μg μmol⁻¹ peptide to allow a better visualization of the

MSNs. Due to the strong fluorescence of DiO, the experiment was repeated with DiO-loaded MSN_{COOH} without the quenching step and using a particle concentration of $150 \mu\text{g} \mu\text{mol}^{-1}$ peptide. The results are shown in **Figure 10**. While the free particles and the $\text{MSN}-\text{PEP}_{\text{RGD}}$ system show roughly equal amounts of particles and DiO inside the cells, the $\text{MSN}-\text{PEP}$ system gave the lowest signal for both components. This suggests that the MSN_{COOH} particles are indeed able to detach from PEP_{RGD} aggregates with time and thus to be taken up by cells. The lower DiO release and particle uptake observed for the $\text{MSN}-\text{PEP}$ system, in combination with the limited adsorption of the PEP fibrillar aggregates to the cells, suggest that the desorption of MSNs from PEP fibrils is kinetically hindered and also that the contribution of dissolved DiO from MSNs cannot account for the very pronounced DiO-originating fluorescence observed for the $\text{MSN}-\text{PEP}_{\text{RGD}}$ system.

2.6. Sequential Addition of PEP_{RGD} and MSN_{COOH} to Cells

Finally, preliminary experiments were carried out to investigate if MSN_{COOH} particles do adsorb to PEP_{RGD} fibrils in the cell

culture medium, that is, in the presence of serum proteins, mimicking a situation where the particles would interact with preformed peptide fibrils *in vitro* and *in vivo* and whose implications this would have on particle uptake and drug delivery to cells. As comparisons, free particles and preformed particle-peptide fibril aggregates were used. The fluorescently labeled MSN_{COOH} carried the DiO dye as a hydrophobic drug model as in the experiments described earlier. Representative fluorescence microscopy images of A549 cells exposed to the administered DiO-containing MSN_{COOH} particles are shown in **Figure 11**.

Interestingly, clearly less particles are present deeper inside the cells in the case when the particles were added after the cells had been exposed to the fibrils, as in the case of free particles and also as compared with particle-fibril coadministration. Furthermore, also in the sequential addition case, most particles are associated with the fibrillar aggregates 24 h postadministration of the particles, highlighting the high preference for the particles to adsorb onto the peptide fibrils and that this interaction is not strongly compromised by the presence of serum proteins.

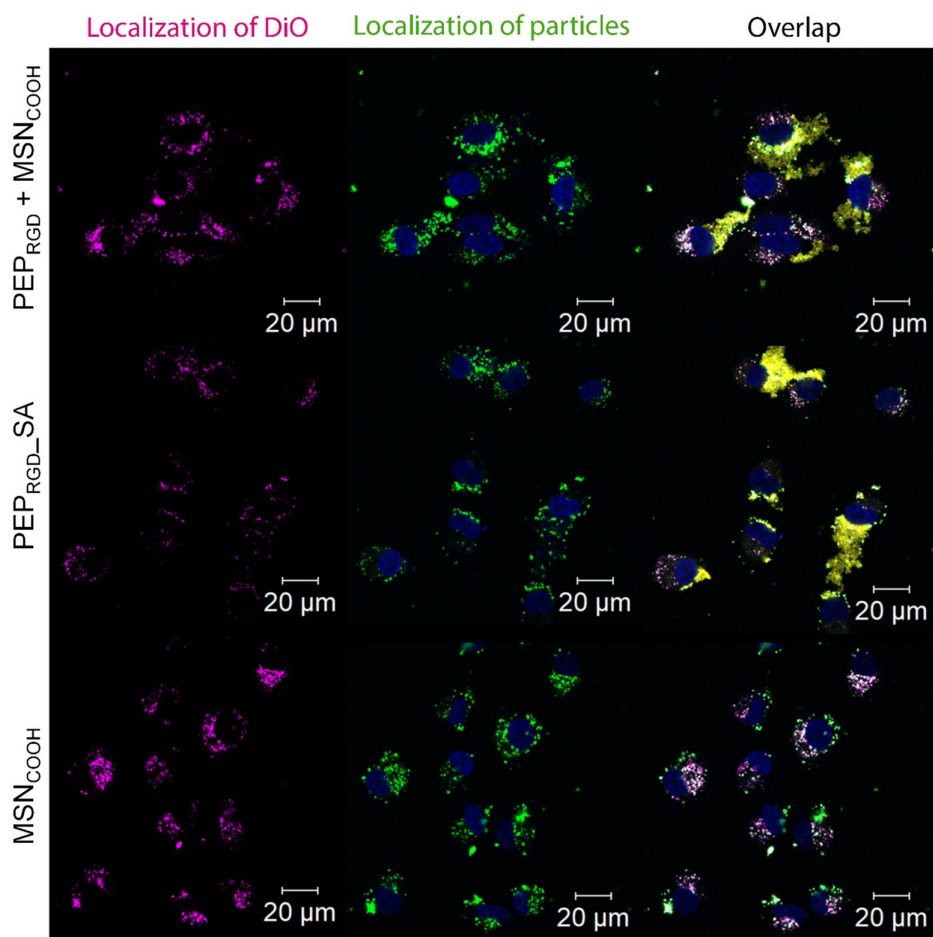


Figure 11. Confocal fluorescence microscopy images of A549 cells exposed to MSNs (green, middle column), releasing the hydrophobic dye DiO (pink, left column) into the cells. The cell nuclei are seen as blue (DAPI staining) and the fibrils with ATTO647N (yellow). Right column, overlay of the two images. The images are taken 24 h after incubating the cells with MSNs carrying DiO. Top: Peptide fibrils preincubated by MSNs before added to the cells, middle: cells have been preincubated by peptide fibrils for 3 h before the MSNs were added, and down: MSNs have been added in free form in the absence of fibrils. $T = 37^\circ\text{C}$.

This can be understood, as we have previously shown that MSN_{COOH} particles adsorb very little serum proteins as compared with purely siliceous MSN particles.^[37] These preliminary results thus suggest that a cellular-targeting strategy based on targetable peptide nanofibrils that first adsorb to target cells followed by administration of nanoparticles that preferentially adsorb to the peptide fibrillary aggregates could be a viable means for targeted drug delivery. Furthermore, as discussed in the introduction, peptide fibrils play an important role in several diseases, and nanoparticles that adsorb strongly to such fibrils can be a viable means for both diagnosing and treating such diseases.

3. Conclusion and Outlook

A modular drug delivery system based on cell-targetable peptide nanofibrils in combination with noncovalently attached MSNs is demonstrated. Our approach presents an entirely new concept for drug delivery based on silica nanoparticles as high-capacity drug transporters and peptide fibrils attached to the cells of interest. It is noteworthy that the concept can also easily be applied to other nanoparticulate drug delivery systems. Intracellular drug delivery following MSN internalization by the cells was demonstrated using a hydrophobic model drug. The extent of diffusion-controlled cargo release is bound to be dependent on the water solubility of the drug. Therefore, it is suggested that such hybrid fibril–particle aggregates are interesting drug delivery systems for local drug delivery of drugs, also in cases where the therapeutic target is extracellular. Examples of the latter are drugging metastatic lymph nodes. Recent studies describe the benefit of the administration of chemotherapy via the lymphatic network through injection of drugs into upstream lymph nodes,^[38] and in such and comparable cases, a prolonged, local drug release from potential even physically trapped hydrogel–nanoparticle carrier systems could be highly beneficial. Furthermore, as the peptide fibrils can serve as drug carriers themselves, combination therapies based on using both fibrils and nanoparticles as drug carriers could open up novel means for efficient, cell-directed drug delivery covering different timescales. Finally, we note that the presented approach is not limited to the large fibrillar aggregates used in this proof-of-concept study but can also be applied for corresponding nanoscopic fibrillar aggregates if an intravenous administration of nanoparticle–fibril aggregates is preferred.

4. Experimental Section

Materials: Diisopropylethylamine (DiPEA), triisopropylsilane chloride (TiPS), tetramethoxysilane (TMOS), (3-aminopropyl)trimethoxysilane (APTMS), *N*-(3-(dimethylamino)propyl)-*N'*-ethylcarbodiimide (EDC), *N*-hydroxysuccinimide (NHS), 3,3'-dioctadecyloxycarbocyanine perchlorate (DiO), cyclohexane, and dichloromethane were obtained from Sigma Aldrich Chemie GmbH (Munich, Germany). Wang resins, Fmoc, and side-chain-protected amino acids, ammonium nitrate and 2-[4-(2-hydroxyethyl)-1-piperazinyl]ethanesulfonic acid sodium salt (HEPES) potassium chloride, were purchased from Merck KGaA (Darmstadt, Germany). Dimethylformamide (DMF), cetyltrimethylammonium bromide (CTAB), methanol, and sodium hydroxide were obtained from VWR International GmbH (Radnor, USA) and ATTO488 and ATTO565 amine from ATTO-TEC GmbH (Siegen, Germany). 2-(1H-benzotriazol-1-yl)-

1,1,3,3-tetramethyluroniumhexafluoro-phosphate (HBTU) was bought at Carbolution Chemicals GmbH (Saarbrücken, Germany) and trifluoroacetic acid (TFA) at Carl Roth GmbH & Co. KG (Karlsruhe, Germany). Dimethylsulfoxide (DMSO), Dulbecco's modified Eagle Medium (DMEM), fetal calf serum (FCS), and Dulbecco's PBS (PBS, without calcium and magnesium) were purchased from Thermo Fisher Scientific Inc. (Waltham, USA). Uranyl acetate was obtained from Serva Electrophoresis GmbH (Heidelberg, Germany) and carboxyethylsilanetriol sodium salt from abcr GmbH (Karlsruhe, Germany). CellTiter-Glo Luminescent Cell Viability Assay was purchased from Promega Corporation (Mannheim, Germany) and Proteostat from Enzo Life Sciences Inc. (Farmingdale, USA).

Peptide Synthesis and Fibril Formation: The peptides were synthesized by standard Fmoc solid-phase peptide synthesis and analyzed by mass spectroscopy. The lyophilized peptides were dissolved in water-free DMSO at a concentration of 10 mg mL⁻¹. Fibril formation was initiated by adding the stock solution into a sodium phosphate buffer (pH 7.0) to obtain a peptide concentration of 0.65 mM and overnight incubation at RT. The verification of the fibrils was done by Proteostat intercalation and electron microscopy. For transelectron microscopy measurements, the fibrils were stained 2 min with 2% uranyl acetate for getting a higher contrast.

Peptide Functionalization: To make the fibrils visible under a fluorescence microscope, they were functionalized with ATTO dyes. Therefore, an ATTO647N-NHS ester stock solution in DMSO (10 mg mL⁻¹) was added to the peptide stock solution in DMSO (10 mg mL⁻¹, 1 μg dye/10 μg) and was rotated for 1 h at room temperature under exclusion of light. The ATTO647N-labeled stock solution was diluted with unlabeled peptide stock solution to gain labeled peptide stock solutions with either 1% or 10% labeled peptides.

Synthesis of Mesoporous Silica Particles: The structure-directing agent cetyltrimethylammonium bromide (CTAB) (7.90 g; 21.7 mmol) was dissolved in a mixture of methanol (640.0 g; 19.98 mol) and water (962.3 g; 53.43 mol). Following complete surfactant dissolution, a soda solution (4.56 mL; 1 M; 4.56 mmol) and a mixture of tetramethylorthosilane (TMOS) (2.18 mL; 13.9 mmol) and aminopropyltrimethylorthosilane (APTMS) (360.0 μL; 1.955 mmol) were added under continuous stirring. The reaction was stirred for another 24 h, after which the particles were flocculated through addition of ammonium nitrate followed by centrifugation. The particles were washed once with water and twice with methanol and dried at 60 °C.

The surfactant was removed from the particles by extraction in an ethanol solution containing ammonium nitrate (6.0 g L⁻¹) for 1 h in an ultrasonic bath. The extraction procedure was repeated three times. The particles were washed twice with methanol and dried at 60 °C.

To obtain all-silica mesoporous particles, the surfactant was removed by calcination at 550 °C for 6 h (heating rate 1 °C min⁻¹). Carboxylic acid-functionalized particles prepared by dispersing calcined silica mesoporous silica particles in HEPES buffer solution (4.0 mg mL⁻¹) and carboxyethylsilanetriol sodium salt (2.0 μL mg⁻¹; 2.9 μmol mg⁻¹) were added. The reaction mixture was rotated for 3 h, followed by particle separation through centrifugation. The particles were washed once with water and two times with ethanol. The resulting carboxylic acid-functionalized particles were dried under vacuum at room temperature.

Fluorescence Labeling of Amino-Functionalized Particles: Amino-functionalized MSN were dispersed in HEPES buffer solution (10 mg mL⁻¹) and an ATTO488-NHS ester stock solution in DMSO (1 mg mL⁻¹; 1.8 μg dye/mg) was added. After rotation for 1 h at room temperature under exclusion of light, the particles were washed three times with methanol and dried under vacuum.

For fluorescence labeling, the carboxylic acid-functionalized particles were dispersed in HEPES buffer solution (10 mg mL⁻¹). For activating the carboxy groups on the surface, EDC (1.7 μL mg⁻¹; 9.6 μmol mg⁻¹) and NHS (1.15 μg mg⁻¹; 9.99 μmol mg⁻¹) were added to the dispersion, which was then rotated for 30 min at room temperature. Thereafter, the particles were centrifuged and washed one time with HEPES buffer solution. The particles were dispersed in HEPES buffer solution (10 mg mL⁻¹) again and ATTO488 amine or ATTO565 amine stock solution in DMSO (1 mg mL⁻¹; 1.8 μg dye/mg) was given to the dispersion, which was then

rotated for 1 h at room temperature under exclusion of light. The particles were washed three times with methanol and dried under vacuum.

Particle Characterization: The size of the particles was analyzed by TEM. Measurements were performed on a Joel 1400 using an acceleration voltage of 120 kV. Determination of the hydrodynamic diameter of the particles was done by dynamic light scattering measurements. These, as well as the zeta-potential measurements, were performed on a Zetasizer Nano-ZS ZEN 3600 from Malvern Instruments using 0.1 mg mL⁻¹ particle dispersions in 1 mM KCl solution (pH = 5.5) and HEPES buffer solution (25 mM; pH = 7.4). For specific surface and pore size distribution, nitrogen sorption measurements were performed at -196 °C on Quadrasorb-SI from Quantachrome Instruments. While the specific surface area was calculated by BET, the pore size and pore volume were determined using the calculation based on the desorption isotherm using the NLDFT kernel developed for silica materials with cylindrical pores. Via thermogravimetric analysis (TGA) on a Netzsch TG209 Libra F1 (heating rate: 10 K min⁻¹), the amount of carboxyl groups on the silica particles was analyzed. Fluorescence properties were examined on a multi-plate reader infinite M1000 from Tecan (ATTO488: $\lambda_{exc} = 450$ nm; $\lambda_{em} = 520$ nm; ATTO565: $\lambda_{exc} = 561$ nm; $\lambda_{em} = 620$ nm).

DiO Loading of the Particles: The adsorbed water was removed by drying the carboxylated particles under vacuum for 3 h at 100 °C. The particles were dispersed in dried cyclohexane (10 mg mL⁻¹) containing the hydrophobic dye DiO (70 µg mg; 75 nmol mg⁻¹). After 24 h rotation at room temperature the particles were separated by centrifugation, washed one time with dried cyclohexane, and dried under vacuum at room temperature. Supernatant and washing cyclohexane were analyzed by UV/vis spectroscopy at NanoDrop 2000c from Thermo Scientific. Concentration of loaded dye was calculated by a calibration curve of DiO in cyclohexane.

On account of the fluorescence properties of DiO for these particles, ATTO565 was used.

Drug Release Experiments: To investigate the drug release behavior of the DiO-loaded particles, they were dispersed in PBS (1 mg mL⁻¹) with pH of 5.0, 6.5, 7.4, and 7.4 with 10% FCS additionally. The dispersions were rotated for 48 h at 37 °C. During the incubation time after 1, 2, 3, 4, 5, 24, and 48 h, 120 µL aliquots were centrifuged. The supernatants from DiO release were fluorescence spectroscopically investigated on a multi-plate reader infinite M1000 from Tecan ($\lambda_{exc} = 475$ nm; $\lambda_{em} = 520$ nm).

Noncovalent Attachment of the Particles to the Fibrils: For the attachment of the particles to the fibrils, a particle stock solution was added to the finished fibrils (150 µg particles/µmol peptide). After 45 min incubation, the attachment was completed. The successful accumulation was verified by electron microscopy, flow cytometry, and confocal microscopy. For transelectron microscopy measurements, the fibrils were stained 2 min with 2% uranyl acetate for getting a higher contrast.

Flow cytometry was used with a new approach where unlabeled fibrils were detected as events instead of normally used cells. Attached ATTO488-labeled MSN_{COOH} led to an increase in fluorescence of the aggregates which can be measured at the flow cytometer.

Cell Culture: Human lung cancer cell line A549 were maintained in DMEM with 10% FCS and 1% penicillin/streptomycin stock solution. The cells were incubated at 37 °C in 5% CO₂. The medium was changed two times a week and the cells passed by trypsination, approximately reaching 75% confluence.

Cell Viability Analysis: Cell viability of the A549 cell line after incubation with the system was investigated using CellTiterGlo assay. A549 cells were cultured in white 96-well microplates with 200 µL medium at a density of 5000 cells per well for 24 h. Pure fibrils (26 µM) and particles (50 µg mL⁻¹) as well as fibril-particle aggregates (26 µM) were added to the cells (40 µL sample filled up to 200 µL with medium) and incubated for 24 and 48 h. After incubation, time medium was removed and 100 µL of a 1:1 diluted CTG stock solution was added to the cells. The cells were incubated for additionally 12 min before measuring the luminescence of each well at Orion Microplate luminometer from Berthold Detection Systems.

Targetability Evaluation in A549 Cell Line: For targetability evaluation, A549 cells were cultured in 8-well ibidi slide with 200 µL medium at a density of 5000 cells per well for 24 h. ATTO488-labeled particles were accumulated to ATTO647N-labeled fibrils (10 mol% labeled). Pure fibrils

(26 µM), pure particles (4.0 µg mL⁻¹), and fibrils with attached particles (26 µM; 150 µg particles/µmol peptide) were given to the cells (40 µL sample filled up to 200 µL with medium) and incubated for 3 h. Subsequently, the cells were rinsed once with the medium and the nuclei were stained with Hoechst for 5 min. The cells were observed under a confocal laser scanning microscope (LSM710 from Zeiss) to capture Hoechst blue fluorescence, ATTO488 green fluorescence, and ATTO647N red fluorescence.

To generate flow cytometry data, A549 cells were cultured in 24-well plates with 2 mL medium at a density of 100 000 cells per well for 24 h. ATTO488-labeled unloaded particles and ATTO647N-labeled fibrils (1 mol% labeled) were used. Particles were attached to the fibrils and were given to the cells (52 µM; 150 µg particles/µmol peptide; 400 µL sample filled up to 2 mL with medium). After 3 h incubation at 37 °C, the cells were washed one time with 1 mL medium and were scrapped from the bottom of the well. The cells were centrifuged for 10 min at 1000 rpm and were resuspended in 100 µL 4% PFA in PBS for fixation of the cells. Before measuring, the cells were diluted with 100 µL PBS and data were generated using a BD FACSCanto II Cell Analyzer from BD Biosciences.

Investigation of the Mechanism of Drug Delivery: For investigation of the mechanism, the A549 cells were treated the same way as for the targetability evaluation, but in this case, the DiO-loaded ATTO565-labeled particles were used. The cells were incubated for 3 h and 24 h at 37 °C, washed once with PBS, and fixed with 4% PFA for 20 min at RT. For measurement and storage at 4 °C, PBS with 1% FCS was given to the cells. The cells were observed under a confocal laser scanning microscope (LSM710 from Zeiss).

To investigate the particle internalization into the cells, the experimental setup was the same than for the targetability evaluation with an increased incubation time of 24 h and a higher particle concentration of 250 µg µmol⁻¹ peptide. The fluorescence of extracellular localized particles was quenched by adding trypan blue (0.5 mg mL⁻¹) for 15 min at RT. After quenching, the cells were washed with PBS and fixed with 4% PFA for 20 min.

The flow cytometric experiments for DiO release into the cells were done the same way as for the targetability evaluation, but in this case, DiO-loaded particles were used and the incubation time was increased up to 24 h.

Investigation of the Sequential Addition: For investigation of the sequential addition of fibrils and MSN, the A549 cells were treated the same way as for the investigation of the mechanism of drug delivery, but in this case in a first step, the fibrils were added to the cells and incubated for 3 h at 37 °C. After that, in a second step, the DiO-loaded ATTO565-labeled particles were added and incubated for another 24 h at 37 °C. The cells were washed once with PBS and fixed with 4% PFA for 20 min at RT. For measurement and storage at 4 °C, PBS with 1% FCS was given to the cells. The cells were observed under a confocal laser scanning microscope (LSM710 from Zeiss).

Supporting Information

Supporting Information is available from the Wiley Online Library or from the author.

Acknowledgements

The authors would like to thank Cornelia Egger (Institute for Inorganic Chemistry II, Ulm University) for nitrogen sorption measurements. The authors gratefully acknowledge the DFG funded CRC 1279 project "Exploiting the human peptidome for novel antimicrobial and anticancer agents" for financial support.

Conflict of Interest

The authors declare no conflict of interest.

Data Availability Statement

The data that support the findings of this study are available from the corresponding author upon reasonable request.

Keywords

drug delivery, nanoparticles, peptide nanofibrils, RGD, silica

Received: September 17, 2021

Revised: November 16, 2021

Published online: December 19, 2021

- [1] Q. Meng, Y. Kou, X. Ma, Y. Liang, L. Guo, C. Ni, K. Liu, *Langmuir* **2012**, *28*, 5017.
- [2] C. J. Bowerman, B. L. Nilsson, *Pept. Sci.* **2012**, *98*, 169.
- [3] S. Lee, T. H. T. Trinh, M. Yoo, J. Shin, H. Lee, J. Kim, E. Hwang, Y.B. Lim, C. Ryou, *Int. J. Mol. Sci.* **2019**, *20*, 5850.
- [4] A. Levin, T. Hakala, L. Schnaider, G. Lopes Bernardes, E. Gazit, T. Knowles, *Nat. Rev. Chem.* **2020**, *4*, 615.
- [5] R. E. Tanzi, L. Bertram, *Cell* **2005**, *120*, 545.
- [6] B. A. Yankner, T. Lu, *J. Biol. Chem.* **2009**, *284*, 4755.
- [7] E. Cerf, A. Gustot, E. Goormaghtigh, J. M. Ruyschaert, V. Raussens, *FASEB J.* **2011**, *25*, 1585.
- [8] D. Easterhoff, J. T. M. DiMaio, T. M. Doran, S. Dewhurst, B. L. Nilsson, *Biophys. J.* **2011**, *100*, 1325.
- [9] J. Münch, E. Rücker, L. Ständker, K. Adermann, C. Goffinet, M. Schindler, S. Wildum, R. Chinnadurai, D. Rajan, A. Specht, G. Giménez-Gallego, P. C. Sánchez, D. M. Fowler, A. Koulou, J. W. Kelly, W. Mothes, J.-C. Grivel, L. Margolis, O. T. Keppler, W.-G. Forssmann, F. Kirchhoff, *Cell* **2007**, *131*, 1059.
- [10] N. R. Roan, N. Sandi-Monroy, N. Kohgadai, S. M. Usmani, K. G. Hamil, J. Neidleman, M. Montano, L. Ständker, A. Röcker, M. Cavois, J. Rosen, K. Marson, J. F. Smith, C. D. Pilcher, F. Gagsteiger, O. Sakk, M. O'Rand, P. V. Lishko, F. Kirchhoff, J. Münch, W. C. Greene, *eLife* **2017**, *6*, e1096.
- [11] D. M. Fowler, A. V. Koulou, C. Alory-Jost, M. S. Marks, W. E. Balch, J. W. Kelly, *PLoS Biol.* **2006**, *4*, 0100.
- [12] S. K. Maji, M. H. Perrin, M. R. Sawaya, S. Jessberger, K. Vadodaria, R. A. Rissman, P. S. Singru, K. P. R. Nilsson, R. Simon, D. Schubert, D. Eisenberg, J. Rivier, P. Sawchenko, W. Vale, R. Riek, *Science* **2009**, *325*, 328.
- [13] J. Gačanin, C. V. Synatschke, T. Weil, *Adv. Funct. Mater.* **2020**, *30*, 1906253.
- [14] M. Yolamanova, C. Meier, A. K. Shaytan, V. Vas, C. W. Bertoncini, F. Arnold, O. Ziraf, S. M. Usmani, J. A. Müller, D. Sauter, C. Goffinet, D. Palesch, P. Walther, N. R. Roan, H. Geiger, O. Lunov, T. Simmet, J. Bohne, H. Schrezenmeier, K. Schwarz, L. Ständker, W.-G. Forssmann, X. Salvatella, P. G. Khalatur, A. R. Khokhlov, T. P. J. Knowles, T. Weil, F. Kirchhoff, J. Münch, *Nat. Nanotechnol.* **2013**, *8*, 130.
- [15] S. Kirti, K. Patel, S. Das, P. Shrimali, S. Samanta, R. Kumar, D. Chatterjee, D. Ghosh, A. Kumar, P. Tayalia, S. K. Maji, *ACS Biomater. Sci. Eng.* **2019**, *5*, 126.
- [16] N. R. Roan, J. Münch, N. Arhel, W. Mothes, J. Neidleman, A. Kobayashi, K. Smith-McCune, F. Kirchhoff, W. C. Greene, *J. Virol.* **2009**, *83*, 73.
- [17] H. D. Herce, A. E. Garcia, J. Litt, R. S. Kane, P. Martin, N. Enrique, A. Rebolledo, V. Milesi, *Biophys. J.* **2009**, *97*, 1917.
- [18] D. Terrone, S. L. W. Sang, L. Roudaia, J. R. Silvius, *Biochemistry* **2003**, *42*, 13787.
- [19] K. Parekh, K. Hariharan, Z. Qu, P. Rewatkar, Y. Cao, M. Moniruzzaman, P. Pandey, A. Popat, T. Mehta, *Int. J. Pharm.* **2021**, *608*, 121079.
- [20] B. Baumann, R. Wittig, M. Lindén, *Nanoscale* **2017**, *9*, 12379.
- [21] V. Mamaeva, C. Sahlgren, M. Lindén, *Adv. Drug Delivery Rev.* **2013**, *65*, 689.
- [22] F. Hoffmann, M. Cornelius, J. Morell, M. Fröba, *Angew. Chem.* **2006**, *118*, 3290.
- [23] Q. He, Z. Zhang, F. Gao, Y. Li, J. Shi, *Small* **2011**, *7*, 271.
- [24] Y. Choi, J. E. Lee, J. H. Lee, J. H. Jeong, J. Kim, *Langmuir* **2015**, *31*, 6457.
- [25] T. I. Janjua, Y. Cao, C. Yu, A. Popat, *Nat. Rev. Mater.* **2021**, *6*, 1072.
- [26] J. M. Rosenholm, A. Meinander, E. Peuhu, R. Niemi, J. E. Eriksson, C. Sahlgren, M. Lindén, *ACS Nano*. **2009**, *3*, 197.
- [27] J. S. Beck, J. C. Vartuli, W. J. Roth, M. E. Leonowicz, C. T. Kresge, K. D. Schmitt, C. T. W. Chu, D. H. Olson, E. W. Sheppard, S. B. McCullen, J. B. Higgins, J. L. Schlenker, *J. Am. Chem. Soc.* **1992**, *114*, 10834.
- [28] T. Mandal, M. Beck, N. Kirsten, M. Lindén, C. Buske, *Sci. Rep.* **2018**, *8*, 2.
- [29] S. Zhang, T. Holmest, C. Lockshin, A. Rich, *Proc. Natl. Acad. Sci.* **1993**, *90*, 3334.
- [30] D. J. Giard, S. A. Aaronson, G. J. Todaro, P. Arnstein, J. H. Kersey, W. P. Parks, *J. Natl. Cancer Inst.* **1973**, *51*, 1417.
- [31] J. M. Rosenholm, E. Peuhu, J. E. Eriksson, C. Sahlgren, M. Lindén, *Nano Lett.* **2009**, *9*, 3308.
- [32] O. Wiltschka, D. Böcking, L. Miller, R. E. Brenner, C. Sahlgren, M. Lindén, *Microporous Mesoporous Mater.* **2014**, *188*, 203.
- [33] E. M. Björk, B. Baumann, F. Hausladen, R. Wittig, M. Lindén, *RSC Adv.* **2019**, *9*, 17745.
- [34] I. Slowing, B. G. Trewyn, V. S. Y. Lin, *J. Am. Chem. Soc.* **2006**, *128*, 14792.
- [35] S. Shahabi, L. Treccani, R. Dringen, K. Rezwan, *ACS Appl. Mater. Interfaces* **2015**, *7*, 13821.
- [36] S. Kralj, M. Rojnik, R. Romih, M. Jagodic, J. Kos, D. Makovec, *J. Nanoparticle Res.* **2012**, *14*, 1151.
- [37] C. Y. Lin, C. M. Yang, M. Lindén, *RSC Adv.* **2019**, *9*, 33912.
- [38] T. Kodama, D. Matsuki, A. Tada, K. Takeda, S. Mori, *Sci. Rep.* **2016**, *6*, 1.